PHYSICAL REVIEW B **89**, 081102(R) (2014)

Second harmonic generation in *h*-BN and MoS_2 monolayers: Role of electron-hole interaction

M. Grüning[1,2] and C. Attaccalite[3]

[1]*School of Mathematics and Physics, Queen's University Belfast, Belfast BT7 1NN, Northern Ireland, United Kingdom*

[2]*Centre for Computational Physics and Physics Department, University of Coimbra, Portugal*

[3]*Université Grenoble Alpes/CNRS, Institut Néel, F-38042 Grenoble, France*

(Received 28 October 2013; published 3 February 2014)

We study second harmonic generation in *h*-BN and MoS_2 monolayers using an *ab initio* approach based on many-body theory. We show that electron-hole interaction doubles the signal intensity at the excitonic resonances with respect to the contribution from independent electronic transitions. This implies that electron-hole interaction is essential to describe second harmonic generation in those materials. We argue that this finding is general for nonlinear optical properties in nanostructures and that the present methodology is the key to disclose these effects.

DOI: 10.1103/PhysRevB.89.081102 PACS number(s): 78.20.Bh, 42.65.Ky, 78.66.−w, 78.67.−n

Introduction. Optical properties of two-dimensional (2D) semiconducting crystals, and specifically of hexagonal boron nitride (*h*-BN) and MoS_2 monolayers, have been the object of intense research in the past years (e.g., Refs. [1–4]). Several studies have investigated the absorption and photoluminescence spectra and possible applications to optoelectronics (for a review see Ref. [5]).

Significant advances in the knowledge of linear optical properties of *h*-BN and MoS_2 have been possible also thanks to *ab initio* studies that contributed both through the interpretation of experimental results (e.g., Refs. [6,7]) and the envisagement of possible applications (e.g., Ref. [8]). Key in those studies has been the inclusion of the electron-hole interaction, essential to capture the excitonic features—particularly strong due to the geometric confinement and the weak dielectric screening—that characterize the optical response of 2D crystals. [9]

More recently, there has been a surge of interest also for nonlinear optical properties of these materials. Several experimental studies [10–12] show that *h*-BN and MoS_2 monolayers have a remarkable second harmonic generation (SHG) hinting at potential applications to nonlinear optical devices. Being sensitive to the stacking, orientation, and number of layers, SHG has been proposed and already used as a noninvasive optical probe to characterize *h*-BN and MoS_2 films [10,11]. On the other hand, as for linear optical properties, it is important to support or even guide experiments through accurate and reliable numerical simulations. As an example, for the MoS_2 monolayer, depending on the study the experimental estimate for the SHG varies by 4 orders of magnitude [10–12].

Unfortunately, in contrast to the case of linear optical properties, calculations of the nonlinear optical response still remain a challenge. With few isolated exceptions [13–15], a large number of calculations of nonlinear optical properties, and specifically of SHG in 2D crystals [16–18], employ the independent-particle approximation (IPA), which is inadequate for low-dimensional systems, where it is expected that the strongly bound excitons significantly modify the SHG.

One of the main obstacles for the inclusion of electron-hole interaction in calculations of nonlinear optical properties actually comes from complexity of the expression for the correlated nonlinear susceptibility in terms of the electronic structure. For example, within many-body perturbation theory the diagrams that enter in the calculation of the second- and third-order susceptibilities are so intricate that their implementation becomes awkward if not impracticable (see for instance Fig. 3 of Ref. [19]). Even within the "simpler" time-dependent density functional theory, equations for the second-order optical response have been solved only for particular approximations for the correlation functional [15] or have been limited to the static response [20].

In a recent work [21], we propose to avoid the direct calculation of the nonlinear optical susceptibilities, and use instead a real-time approach. In such an approach the optical susceptibilities are obtained from the time propagation of "simpler" objects such as the single-particle Green's function, the density matrix, or the density. Many-body effects then are included easily as an operator into the time-dependent (effective) Hamiltonian. This approach has been already successfully implemented and used for example within time-dependent density functional theory, but usually limited to finite systems, such as atoms, molecules, or clusters [22]. Our approach is instead designed to treat periodic systems, such as crystals, and is based on an approximation for the electron-hole interaction [23] derived from many-body perturbation theory that proved to be successful for linear optical properties (e.g., Refs. [6,7]).

Here we apply this approach to calculate and analyze the contribution of electron-hole interaction on the SHG spectra of *h*-BN and MoS_2 monolayers. For both materials we disclose the signature of bound excitons and show that excitonic effects not only significantly modify the shape of the spectrum with respect to the IPA, but strongly enhance its intensity. In the conclusions we comment how this finding may open the possibility of engineering the SHG signal in these materials.

Computational methods. The main equation in our real-time approach to nonlinear optical properties is the equation of motion for the time-dependent valence states $|v_{\mathbf{k},m}\rangle$:

$$i\hbar\frac{d}{dt}|v_{\mathbf{k},m}\rangle = (H^0_{\mathbf{k}} + \Delta H_{\mathbf{k}} + V_h[\Delta\rho] + \Sigma_{\mathrm{SHF}}[\Delta\gamma])|v_{\mathbf{k},m}\rangle + \boldsymbol{\mathcal{E}}|\partial_{\mathbf{k}} v_{\mathbf{k},m}\rangle, \quad (1)$$

where $\Delta\rho(\mathbf{r}) = \rho(\mathbf{r};t) - \rho(\mathbf{r};t=0)$ and $\Delta\gamma = \gamma(\mathbf{r},\mathbf{r}';t) - \gamma(\mathbf{r},\mathbf{r}';t=0)$ are respectively the variation of the electronic density and of density matrix induced by the external field $\boldsymbol{\mathcal{E}}$. The last term on the right-hand side of Eq. (1) describes

the coupling with the external field. We treat this term within the modern theory of polarization [24] in the extension to dynamical polarization proposed by Souza *et al.* [25] that we recently implemented in an *ab initio* framework [21].

The rest of the terms on the right-hand side correspond to different approximations for the effective Hamiltonian. The first term $H^0_{\mathbf{k}}$ is the unperturbed mean-field Hamiltonian, for which we choose the Kohn-Sham one [26] and corresponds to the IPA. The second term, $\Delta H_{\mathbf{k}}$, is the so-called scissor operator that corrects the band structure of $H^0_{\mathbf{k}}$ to provide the quasiparticle band structure. Here the scissor is evaluated within the GW approximation [27] and the corresponding approximation referred as IPA + GW corrections. The third term, $V_h(\mathbf{r})[\Delta\rho]$, is the Hartree [28] potential. This term is responsible for the local-field effects [29] originating from system inhomogeneities. By truncating Eq. (1) at this level one obtains the time-dependent Hartree (TDH) approximation. The next term in Eq. (1) is the screened Hartree-Fock (SHF) self-energy Σ_{SHF}, which accounts for the electron-hole interaction [23], and is written as $\Sigma_{\text{SHF}}[\Delta\gamma] = W(\mathbf{r},\mathbf{r}')\Delta\gamma(\mathbf{r},\mathbf{r}';t)$, where the static screened Coulomb interaction $W(\mathbf{r},\mathbf{r}')$ is calculated in random phase approximation keeping the screening fixed to its zero-field value (for details see Ref. [28]). Approximation at this level is referred as time-dependent SHF (TDSHF). Note that within Green's function theory the linear response limit of the full Eq. (1) is equivalent to the solution of the Bethe-Salpeter equation [23] in the static ladder approximation on top of the G_0W_0 quasiparticle band structure [27].

In order to calculate the nonlinear optical response to an external field, we choose a monochromatic (sinusoidal) electric field in Eq. (1), and calculate the time-dependent polarization as

$$\mathbf{P}_{\parallel} = -\frac{ef}{2\pi v}\frac{\mathbf{a}}{N_{\mathbf{k}_\perp}}\sum_{\mathbf{k}_\perp}\text{Im}\log\prod_{\mathbf{k}_{\parallel}}^{N_{\mathbf{k}_{\parallel}}-1}\det S(\mathbf{k},\mathbf{k}+\mathbf{q}_{\parallel}), \qquad (2)$$

where $\mathbf{P}_{\parallel}$ is the polarization along the lattice vector $\mathbf{a}$, v is the unit cell volume, $S(\mathbf{k},\mathbf{k}+\mathbf{q}_{\parallel})$ is the overlap matrix between the time-dependent valence states $|v_{\mathbf{k},n}\rangle$ and $|v_{\mathbf{k}+\mathbf{q}_{\parallel},m}\rangle$, $N_{\mathbf{k}_{\parallel}}$ and $N_{\mathbf{k}_\perp}$ are respectively the number of k points along and perpendicular to the polarization direction, and $\mathbf{q}_{\parallel} = \frac{\mathbf{b}}{N_{\mathbf{k}_{\parallel}}}$ (with $\mathbf{b}$ the primitive reciprocal lattice vector such that $\mathbf{b}\cdot\mathbf{a} = 2\pi$). The second harmonic coefficient is extracted from the power series of total polarization $P = \chi^{(1)}\mathcal{E} + \chi^{(2)}\mathcal{E}\mathcal{E} + \cdots$ as explained in more detail in Ref. [21].

We apply the method here reviewed to h-BN [30] and MoS_2 [31] monolayers. Valence states are expanded in a plane-wave basis set and the isolated monolayers are simulated by a slab supercell approach with large intersheet distance. Numerical details can be found in Refs. [30–32].

h-BN monolayer. h-BN is a transparent insulating material with a large band gap of about 6 eV. Its absorption spectrum is dominated by strong bound excitons, nearly independent from the layers arrangement [7,33]. The h-BN monolayer inherits all these properties from its bulk counterpart.

In Fig. 1 we report the calculated absolute value of $\chi^{(2)}_{aab}(\omega)$, the only independent in-plane component of $\chi^{(2)}(\omega)$ (a and b are the in-plane Cartesian directions) at different levels of approximation. Assignment of the peak is done by comparison

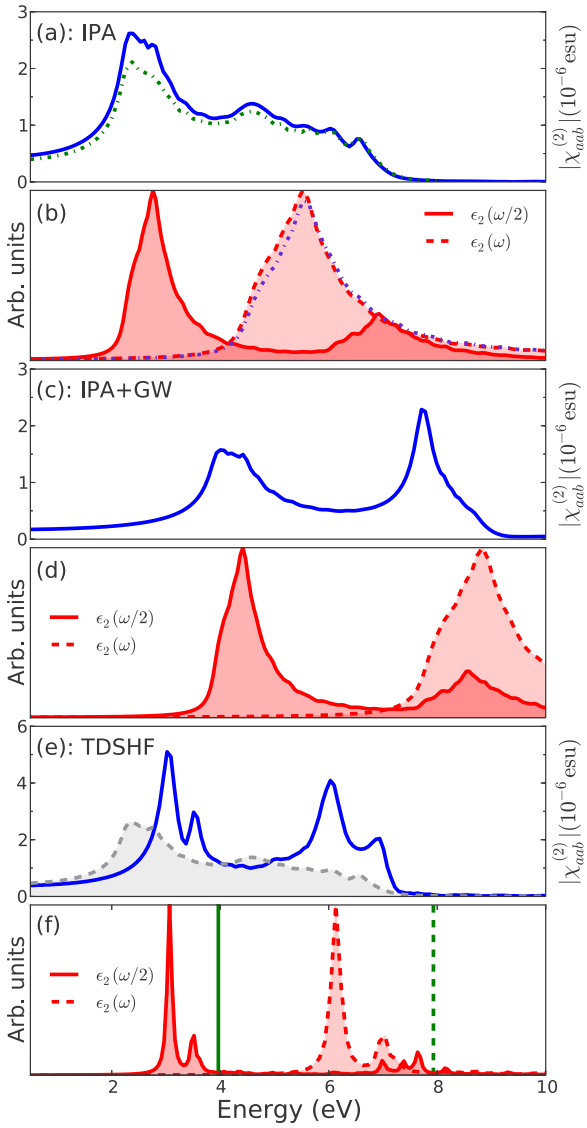

FIG. 1. (Color online) SHG spectra for the h-BN monolayer at different levels of theory [Eq. (1)]: (a) IPA (blue continuous line) and TDH (green dashed line); (c) IPA + GW correction (blue continuous line); (e) TDSHF (blue continuous line) and IPA (gray dashed line). The imaginary part of the dielectric constant at both $\omega/2$ (red continuous line) and ω (red dashed line) is reported in (b), (d), and (f) for IPA, TDH, and TDSHF, respectively. The vertical lines represent the GW fundamental gap (green dashed line) and half of the GW fundamental gap (green continuous line).

with the imaginary part of the independent-particle dielectric constant ϵ_2 [Figs. 1(b), 1(d), and 1(f)]. At IPA level [Fig. 1(a)], the SHG presents a peak at 2.3 eV and a broad structure between 4 and 7 eV, corresponding respectively to two-photon and one-photon resonances with $\pi \to \pi^*$ transitions, with contributions around 7 eV of two-photon resonances with $\sigma \to \sigma^*$ transitions. The IPA level of theory is the one usually employed in theoretical calculations of SHG. Results for the h-BN monolayer were previously obtained by Guo and Lin [16] and are in good agreement with our calculations (see also Table I). In the following we show how effects beyond the IPA—that is, the additional terms in Eq. (1)—modify the SHG spectrum.

TABLE I. $\omega \to 0$ limit of $\chi^{(2)}_{aab}(-2\omega,\omega,\omega)$ of the h-BN monolayer at different levels of the theory [Eq. (1)]. As a comparison, for the IPA we report in square brackets also the value obtained in Ref. [16].

$\chi^{(2)}_{aab}(0)$ (pm/V)	IPA		TDH	IPA + G_0W_0	TDSHF
h-BN	41.2(7)	[40.7]	34.7(9)	16.8(1)	36.8(3)

We start by adding crystal local field effects included at the TDH level [Fig. 1(a)]. Because of the weak in-plane inhomogeneity of the h-BN, local field effects are small and reduce by about 20% the peak at 2.3 eV. Note however that they are larger than in the absorption spectrum for which the effect is negligible [Fig. 1(b)]. Next we consider the renormalization of the band structure by quasiparticle corrections within the GW approximation (IPA + GW) [Fig. 1(c)]. For h-BN this renormalization can be safely approximated by a rigid shift of the conduction bands [30]. Differently from the absorption spectrum [Fig. 1(d)], the SHG is not simply shifted by GW corrections, but its shape changes remarkably as a consequence of the more involved pole structure of the second-order susceptibility [15,34]. In fact, the IPA + GW shows two peaks: the first at about 4 eV is the shifted two-photon $\pi \to \pi^*$ resonances peak which is attenuated by 40% with respect to IPA [Fig. 1 (a)]; the second very pronounced peak at about 8 eV comes from the interference of $\pi \to \pi^*$ one-photon resonances and $\sigma \to \sigma^*$ two-photon resonances.

Finally, in Fig. 1(e) we consider the full Hamiltonian in Eq. (1). In particular we add the SHF term that introduces an attractive interaction between the excited electrons and holes [23]. The SHG spectrum presents four sharp and strong peaks and its onset is redshifted by about 1 eV with respect to the the IPA + GW [Fig. 1(c)]. The two couples of peaks can be identified respectively as the two- and one-photon resonances with the excitons at 6 and 7 eV. Figure 1(c) also emphasizes the striking difference with respect to IPA, and shows that TDSHF is twice as strong as IPA at the exciton resonances. In Table I we report the value of the second optical susceptibility at $\omega = 0$, $\chi^{(2)}(\omega \to 0)$, extrapolated from the SHG behavior at small frequencies. Again, at the IPA level our result agrees with the one of Guo and Lin [16] within the error bar. Adding the effects beyond IPA modifies the $\chi^{(2)}(\omega \to 0)$ value, and in particular within TDSHF we found a value smaller by about 10% than within IPA. Experimentally, Ref. [11] provides an estimate for the SHG at 1.53 eV (810 nm) (assuming an effective layer thickness of 3.3 Å) of about 5×10^{-8} esu, one order of magnitude smaller than what we find, though a direct quantitative comparison is difficult since experiments measure the second harmonic signal of the monolayer relative to the underlying substrate.

MoS_2 monolayer. MoS_2 differs from h-BN in several aspects. First, in MoS_2 an indirect-to-direct band gap transition occurs passing from the bulk to the monolayer due to the vanishing interlayer interaction. Second, spin-orbit coupling plays an important role in this material, splitting the top valence bands, as visible from the absorption spectrum, presenting a double peak at the onset [2]. Third, Mo and S atoms in the MoS_2 monolayer are on different planes resulting in a larger inhomogeneity than for the h-BN.

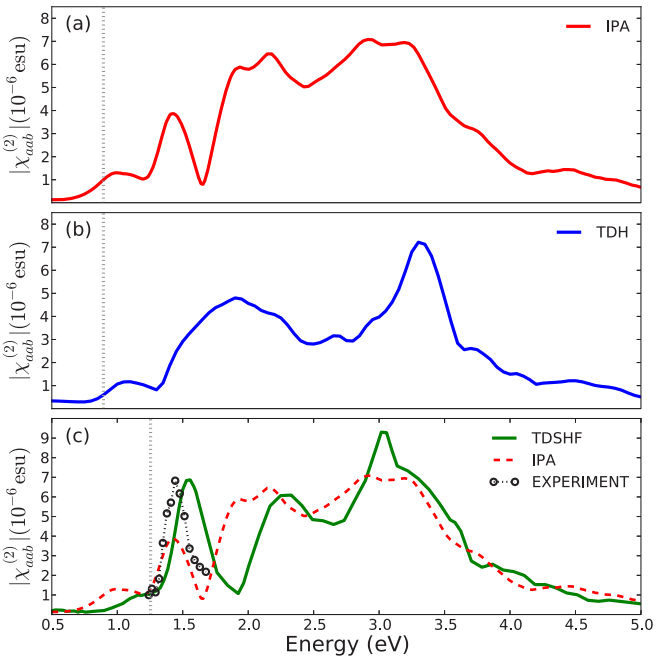

FIG. 2. (Color online) SHG in the MoS_2 monolayer for different approximations: (a) IPA, (b) TDH, and (c) TDSHF (green line). The latter is compared with IPA (red dashed line) and experimental results of Malard *et al.* [12] (black circles). The intensity of the experimental spectrum has been renormalized to match the intensity of the 1.5 eV peak (see text). The dotted vertical lines show the energy of half of the Kohn-Sham band gap in (a) and (b), and of half of the GW band gap in (c).

Figure 2 presents the SHG spectra $|\chi^{(2)}_{aab}|$ of the MoS_2 monolayer at the different levels of approximations of Eq. (1). At the IPA level [Fig. 2(a)], the SHG presents three main features: a small peak at 1 eV, which originates from two-photon resonances with transitions close to the minimum gap at the K point; a larger peak around 1.5 eV, which originates from two-photon resonances with transitions along the high-symmetry axis between Γ and K where the highest valence and lowest conduction bands are flat and there is a high density of states; and a broad structure between 2–3.5 eV which originates from one-photon resonances with transitions at K and along Γ-K and two-photon resonances with transitions at higher energies. Note that we do not include spin-orbit coupling in Eq. (1). The latter is expected to split the lowest peak into two weaker subpeaks [6] but to leave unaffected the second peak, the one observed experimentally [12].

Because of the inhomogeneity of the MoS_2 monolayer the addition of crystal local field effects within the TDH strongly modifies the SHG [Fig. 2(b)]. In particular the main peak at 1.5 eV merges with the plateau at 2 eV while a peak appears around 3.3 eV. Finally, within the TDSHF [Fig. 2(c)] the small shoulder around 1 eV, below half of the GW gap (1.25 eV, gray dotted vertical line in the figure), originates from two-photon resonances with the bound excitons around 2 eV which are well visible in the experimental absorption spectra [2]. The main peak at about 1.5 eV, present in the IPA spectrum but washed out by local field effects within the TDH, is restored by the electron-hole interaction and its intensity is two times larger

than in the IPA case. This peak corresponds to a two-photon resonance with the bright exciton at 3 eV observed in the absorption spectrum [6,12]. The calculated spectrum also shows a strong one-photon resonance with the same exciton at 3 eV.

Interestingly the two-photon resonance with the bright exciton at 3 eV falls into the wavelength range of Ti:sapphire lasers. In fact it has been measured recently in different experiments [10–12] reporting estimates for the SHG at 810 nm (1.53 eV) ranging over 4 orders of magnitude. In Fig. 2(c) we compare the TDSHF-calculated spectrum with the experimental measurements of Malard *et al*. [12] between 1.2 and 1.7 eV, finding a good agreement for the position and shape of the peak at about 1.5 eV. The calculated intensity is one order of magnitude larger (about a factor 21) than the experimental estimate from both Refs. [11,12] (assuming an effective layer thickness of 6.2 Å). On the other hand our value is smaller by 2–3 orders of magnitude than the experimental estimate reported in Ref. [10]. The same differences between theoretical and experimental SHG have been also reported recently by Trolle and coworkers [18] that calculated the SHG of the MoS_2 monolayer in the IPA from a tight-binding band structure. As in the case of *h*-BN, a quantitative comparison with experiment is however difficult: in the experiment the second harmonic signal from the monolayer is measured relative to the underlying substrate and assumptions are made to deduce its absolute value. On the other hand in our calculations we neglect effects that may be relevant such as the reflection of the fundamental and second harmonic field from the substrate. We note finally that our calculations predict the difference of one order of magnitude between the SHG in MoS_2 and *h*-BN at 810 nm (1.53 eV) as reported in Ref. [11].

To summarize, we have shown that electron-hole interaction greatly enhances the SHG signal in 2D crystals with respect to the independent-particle picture. Specifically, for the *h* -BN monolayer one- and two-photon resonances with bound excitons produce strong signatures in the SHG spectrum with intensities two times larger than expected from the IPA. In MoS_2, though the shape of the spectrum is not strikingly modified by excitonic effects as for *h*-BN, the electron-hole interaction enhances, again by about 200%, the SHG signal in the visible range with respect to the IPA.

This finding may provide a spin-off for the quest of materials with high SHG. In fact—given that the SHG signal depends largely on the electron-hole interaction that in turn depends on the electronic screening—the SHG intensity can be tuned by changing the electronic screening. Then, it may be possible, as proposed in Ref. [35], to engineer metamaterials with a high SHG by combining layers of different 2D crystals [35] so as to change the electronic screening, and further enhance the electron-hole interaction effects.

As a side finding, our results emphasize that it is critical for theoretical and computational approaches to accurately include electron-hole interaction, together with quasiparticle and local field effects, in order to predict nonlinear optical response in low-dimensional materials. In this regard, our recently proposed approach [21,28] is quite promising as it imports into the very flexible real-time framework—apt to treat nonlinear optics—the combination of BSE + GW successfully applied to the linear optical response of low-dimensional materials.

Acknowledgments. The authors thank L. Stella and J. Kohanoff for a critical reading of the manuscript, and X. Blase for computational resources. M.G. acknowledges the Portuguese Foundation for Science and Technology for funding (PTDC/FIS/103587/2008) and support through the Ciência 2008 program. Computing time has been provided by the national GENGI-IDRIS supercomputing centers, Contract No. i2012096655.

[1] A. Splendiani *et al*., Nano Lett. **10**, 1271 (2010).
[2] K. F. Mak, C. Lee, J. Hone, J. Shan, and T. F. Heinz, Phys. Rev. Lett. **105**, 136805 (2010).
[3] Y. Kubota, K. Watanabe, O. Tsuda, and T. Taniguchi, Science **317**, 932 (2007).
[4] K. Watanabe, T. Taniguchi, and H. Kanda, Nat. Mater. **3**, 404 (2004).
[5] G. Eda and S. A. Maier, ACS Nano **7**, 5660 (2013).
[6] A. Molina-Sánchez, D. Sangalli, K. Hummer, A. Marini, and L. Wirtz, Phys. Rev. B **88**, 045412 (2013).
[7] L. Wirtz, A. Marini, M. Grüning, C. Attaccalite, G. Kresse, and A. Rubio, Phys. Rev. Lett. **100**, 189701 (2008).
[8] M. Bernardi, M. Palummo, and J. C. Grossman, Nano Lett. **13**, 3664 (2013).
[9] G. D. Scholes and G. Rumbles, Nat. Mater. **5**, 683 (2006).
[10] N. Kumar, S. Najmaei, Q. Cui, F. Ceballos, P. M. Ajayan, J. Lou, and H. Zhao, Phys. Rev. B **87**, 161403 (2013).
[11] Y. Li *et al*., Nano Lett. **13**, 3329 (2013).
[12] L. M. Malard, T. V. Alencar, A. M. Barboza, K. F. Mak, and A. M. de Paula, Phys. Rev. B **87**, 201401 (2013).
[13] R. Leitsmann, W. G. Schmidt, P. H. Hahn, and F. Bechstedt, Phys. Rev. B **71**, 195209 (2005).
[14] E. K. Chang, E. L. Shirley, and Z. H. Levine, Phys. Rev. B **65**, 035205 (2001).
[15] E. Luppi, H. Hübener, and V. Véniard, Phys. Rev. B **82**, 235201 (2010).
[16] G. Y. Guo and J. C. Lin, Phys. Rev. B **72**, 075416 (2005).
[17] V. A. Margulis, E. Muryumin, and E. Gaiduk, J. Phys.: Condens. Matter **25**, 195302 (2013).
[18] M. L. Trolle, G. Seifert, and T. G. Pedersen, arXiv:1310.0674.
[19] K. S. Virk and J. E. Sipe, Phys. Rev. B **80**, 165318 (2009).
[20] B. Kirtman, F. L. Gu, and D. M. Bishop, J. Chem. Phys. **113**, 1294 (2000).
[21] C. Attaccalite and M. Grüning, Phys. Rev. B **88**, 235113 (2013).
[22] Y. Takimoto, F. D. Vila, and J. J. Rehr, J. Chem. Phys. **127**, 154114 (2007).
[23] G. Strinati, Riv. Nuovo Cimento **11**, 1 (1988).
[24] R. Resta, Rev. Mod. Phys. **66**, 899 (1994).
[25] I. Souza, J. Íñiguez, and D. Vanderbilt, Phys. Rev. B **69**, 085106 (2004).
[26] W. Kohn and L. J. Sham, Phys. Rev. **140**, A1133 (1965).
[27] W. G. Aulbur, L. Jönsson, and J. W. Wilkins, in *Solid State Physics*, Vol. 54, edited by H. Ehrenreich and F. Spaepen (Elsevier, Amsterdam, 1999), p. 1.

[28] C. Attaccalite, M. Grüning, and A. Marini, Phys. Rev. B **84**, 245110 (2011).

[29] S. L. Adler, Phys. Rev. **126**, 413 (1962).

[30] For the hexagonal BN we used a lattice constant of $a = 2.52$ Å, and an interlayer distance of 20 a.u. The electron-ion term was approximated using norm-conserving pseudopotentials and an exchange correlation term using the local density approximation. The GW correction of 3.3 eV was taken from Refs. [7, 33]. The screened Coulomb interaction was calculated using 30 bands and a cutoff of 2 Ha on the dielectric matrix dimensions. SHG was obtained using 8 bands: 4 valence and 4 conduction. Within IP and TDH we used a $40 \times 40 \times 1k$-point grid, within TDSHF the optical spectra is dominated by a strongly bound exciton, and a $14 \times 14 \times 1k$-point grid is sufficient to converge the spectra.

[31] For the MoS_2 layer we used the experimental lattice constant of the bulk MoS_2 as in Ref. [6] and an interlayer distance of 30 a.u. The electron-ion term was approximated using norm-conserving pseudopotentials and an exchange correlation term using the Perdew, Burke, and Ernzerhof functional [J. P. Perdew, K. Burke, and M. Ernzerhof, Phys. Rev. Lett. **77**, 3865 (1996)]. The GW correction of 0.72 eV was taken from Ref. [6]. The screened Coulomb interaction was calculated using 100 bands and a cutoff of 2 Ha on the dielectric matrix dimensions. SHG was obtained using a $21 \times 21 \times 1k$-point grid, 18 bands within IPA and TDH, and bands between the 3rd and the 16th for the TDSHF.

[32] Calculations of $H^0_{\mathbf{k}}$ are performed with ABINIT [36], while Eq. (1) is solved using a development version of the YAMBO code [37], where also Eq. (2) has been implemented. Equation (1) is numerically integrated with a time step of $\Delta t = 0.0025$ fs, that guarantees accuracy and stable results. In order to reproduce experimental conditions we use a laser intensity of $I = 500$ kW/cm^2. In Eq. (1) we add a dephasing term with $\tau = 6$ fs to simulate a finite broadening of about 0.2 eV [21], and propagate for 55 fs for each laser frequency.

[33] L. Wirtz, A. Marini, and A. Rubio, Phys. Rev. Lett. **96**, 126104 (2006).

[34] J. L. P. Hughes and J. E. Sipe, Phys. Rev. B **53**, 10751 (1996).

[35] G. Gao *et al.*, Nano Lett. **12**, 3518 (2012).

[36] X. Gonze *et al.*, Comput. Mater. Sci. **25**, 478 (2002).

[37] A. Marini, C. Hogan, M. Gruning, and D. Varsano, Comput. Phys. Commun. **180**, 1392 (2009).